PROCEEDINGS OF SCIENCE

Measurement of CP violating phase ϕ_s at CMS

Fabrizio Palla[*†]
INFN Sezione di Pisa
E-mail: Fabrizio.Palla@cern.ch

I will present the measurements of the CP-violating phase ϕ_s and the decay width difference $\Delta\Gamma_s$ between the two B_s^0 mass eigenstates performed by the CMS collaboration during the first run of LHC and discuss their prospects using the data collected in Run2 (2015-2018). The estimate for the high-luminosity phase of the LHC (HL-LHC) will be finally discussed.

18th International Conference on B-Physics at Frontier Machines - Beauty2019 -
29 September / 4 October, 2019
Ljubljana, Slovenia

[*]Speaker.
[†]On behalf of the CMS Collaboration

PoS(Beauty2019)004

1. Introduction

The CP-violating weak phase ϕ_s arises from the interference between direct $B_s^0 \to J/\psi\phi$ meson decay amplitude and its decay via the $\overline{B_s^0}$ mixed amplitude. In the Standard Model (SM) it is related to the CP-violating phase of the B_s^0 unitarity CKM triangle, $\phi_s \approx -2\beta_s = \arg\left(-\frac{V_{ts}V_{tb}^*}{V_{cs}V_{cb}^*}\right)$[1]. Its numerical value is determined via a global fit to available experimental data to be $2\beta_s = (36.96^{+0.84}_{-0.72}$ mrad)[2]. Any deviation of the measured value from the SM prediction imply presence of new physics processes. The two B_s^0 mass eigenstates are approximately equal to the CP eigenstates, due to the smallness of the CP-violation in the SM, and their decay width difference $\Delta\Gamma_s$ can also be measured from their lifetimes. In the following I will present the measurements performed by the CMS collaboration at the LHC using data collected in the first run of LHC (Run1) [3] and discuss their prospects with the collected data in Run2 (2015-2018). Finally I will discuss the estimate for the high-luminosity phase of the LHC (HL-LHC).

2. Ingredients for the analysis

The measurement is performed by a time dependent angular analysis of the differential decay rate of tagged and untagged $B_s^0 \to J/\psi\phi$ events [4]:

$$\frac{\mathrm{d}^4\Gamma}{\mathrm{d}\Theta\mathrm{d}t} = f(\Theta,t,\alpha) \propto \sum_{i=1}^{10} \varepsilon(\Theta)\varepsilon(t)\tilde{O}_i(\alpha,t)g_i(\Theta) \tag{2.1}$$

$$\tilde{O}_i(\alpha,t) = \int O_i(\alpha,t')\mathrm{R}(\mathrm{t}-\mathrm{t}')\mathrm{d}t'$$

where O_i are time dependent functions, R the per-event time resolution function, g_i are angular functions, and α a set of parameters

$$\alpha = \left\{\Delta\Gamma_s, c\tau, \Delta\mathrm{m_s}, |\mathrm{A_0}|^2, |\mathrm{A_\perp}|^2, |\mathrm{A_\parallel}|^2, |\mathrm{A_S}|^2, \delta_\parallel, \delta_\perp, \delta_\mathrm{S}, \delta_0\right\}. \tag{2.2}$$

Experimentally, the time dependent functions O_i describe the evolution of the decay rates of initially produced B_s^0 diluted by the presence of an initial flavour tag ($\xi = 0, \pm 1$) and its corresponding fraction of mistag (ω)[4]:

$$O_i(\alpha,t) = N_i e^{-ict/c\tau}\left[a_i \cosh\left(\frac{\Delta\Gamma_s}{2}t\right) + b_i \sinh\left(\frac{\Delta\Gamma_s}{2}t\right) + c_i\xi(1-2\omega)\cos(\Delta m_s t) + d_i\xi(1-2\omega)\sin(\Delta m_s t)\right]. \tag{2.3}$$

The equation for $\overline{B_s^0}$ is obtained by changing the sign of the c_i and d_i terms. The parameters $|A_0|^2, |A_\perp|^2$ and $|A_\parallel|^2$ are the magnitude squared of the longitudinal, perpendicular, and parallel $P-$wave amplitudes, respectively; $|A_S|^2$ is the magnitude squared of the $S-$wave amplitude representing the fraction of non-resonant decays $B_s^0 \to J/\psi K^+K^-$; the parameters $\delta_\parallel, \delta_\perp, \delta_S, \delta_0$ are their corresponding strong phases. The terms N_i, a_i, b_i, c_i, d_i are given in Table 2. The coefficients b_i and d_i are sensitive to $\cos(\phi_s)$ and $\sin(\phi_s)$; it is worth noting that also untagged events ($\xi = 0$) contribute.

The analysis is performed using an integrated luminosity of 19.7 fb^{-1} collected at a centre-of-mass energy of $\sqrt{s} = 8$ TeV in proton-proton collisions at LHC during 2011 and 2012. Events are

i	$g_i(\theta_T, \psi_T, \varphi_T)$	N_i	a_i	b_i	c_i	d_i
1	$2\cos^2\psi_T(1-\sin^2\theta_T\cos^2\varphi_T)$	$\lvert A_0(0)\rvert^2$	1	D	C	$-S$
2	$\sin^2\psi_T(1-\sin^2\theta_T\sin^2\varphi_T)$	$\lvert A_\parallel(0)\rvert^2$	1	D	C	$-S$
3	$\sin^2\psi_T\sin^2\theta_T$	$\lvert A_\perp(0)\rvert^2$	1	$-D$	C	S
4	$-\sin^2\psi_T\sin 2\theta_T\sin\varphi_T$	$\lvert A_\parallel(0)\rvert\lvert A_\perp(0)\rvert$	$C\sin(\delta_\perp-\delta_\parallel)$	$S\cos(\delta_\perp-\delta_\parallel)$	$\sin(\delta_\perp-\delta_\parallel)$	$D\cos(\delta_\perp-\delta_\parallel)$
5	$\frac{1}{\sqrt{2}}\sin 2\psi_T\sin^2\theta_T\sin 2\varphi_T$	$\lvert A_0(0)\rvert\lvert A_\parallel(0)\rvert$	$\cos(\delta_\parallel-\delta_0)$	$D\cos(\delta_\parallel-\delta_0)$	$C\cos(\delta_\parallel-\delta_0)$	$-S\cos(\delta_\parallel-\delta_0)$
6	$\frac{1}{\sqrt{2}}\sin 2\psi_T\sin 2\theta_T\sin\varphi_T$	$\lvert A_0(0)\rvert\lvert A_\perp(0)\rvert$	$C\sin(\delta_\perp-\delta_0)$	$S\cos(\delta_\perp-\delta_0)$	$\sin(\delta_\perp-\delta_0)$	$D\cos(\delta_\perp-\delta_0)$
7	$\frac{2}{3}(1-\sin^2\theta_T\cos^2\varphi_T)$	$\lvert A_S(0)\rvert^2$	1	$-D$	C	S
8	$\frac{1}{3}\sqrt{6}\sin\psi_T\sin^2\theta_T\sin 2\varphi_T$	$\lvert A_S(0)\rvert\lvert A_\parallel(0)\rvert$	$C\cos(\delta_\parallel-\delta_S)$	$S\sin(\delta_\parallel-\delta_S)$	$\cos(\delta_\parallel-\delta_S)$	$D\sin(\delta_\parallel-\delta_S)$
9	$\frac{1}{3}\sqrt{6}\sin\psi_T\sin 2\theta_T\cos\varphi_T$	$\lvert A_S(0)\rvert\lvert A_\perp(0)\rvert$	$\sin(\delta_\perp-\delta_S)$	$-D\sin(\delta_\perp-\delta_S)$	$C\sin(\delta_\perp-\delta_S)$	$S\sin(\delta_\perp-\delta_S)$
10	$\frac{4}{3}\sqrt{3}\cos\psi_T(1-\sin^2\theta_T\cos^2\varphi_T)$	$\lvert A_S(0)\rvert\lvert A_0(0)\rvert$	$C\cos(\delta_0-\delta_S)$	$S\sin(\delta_0-\delta_S)$	$\cos(\delta_0-\delta_S)$	$D\sin(\delta_0-\delta_S)$

Table 1: Angular and time-dependent terms of the signal model.

triggered using two opposite charge muons with a $p_T > 4$ GeV with an invariant mass within 200 MeV from the J/ψ mass, a decay length significance in the transverse plane larger than 3 and a pointing angle smaller than 0.45 rad.

The offline reconstruction refines the two muons invariant mass cut to 150 MeV; the ϕ is reconstructed by requiring two opposite charge tracks with $p_T > 700$ MeV forming an invariant mass within 10 MeV from the ϕ mass. The two muons and the two tracks are requested to form a vertex with a confidence level fit larger than 2%, an invariant mass within 120 MeV from the B_s^0 mass and a decay length between 0.02 and 3 cm. About 49 thousand events are selected. The main background for the signal events originates from non-prompt J/ψ mesons from other B hadron decays.

The initial flavour tag is determined by using a multi-layered perceptron neural network (MLP-NN) that used properties of reconstructed opposite-side electrons and muons. The MLP-NN is trained on Monte Carlo signal events to separate right from wrong tagged events. The tagging algorithm is optimised by maximising the tagging power $\varepsilon_{tag}(1-2\omega)^2$, which represents the equivalent efficiency of a sample with perfect tagging ($\omega = 0$). The term ε_{tag} is the tagging efficiency, defined as the fraction of events to which a tag decision is found by the tagging algorithm. About 700 thousands $B^\pm \to J/\psi K^\pm$ self-tagged reconstructed data events are used to obtain mistag probabilities, where the charge of the reconstructed Kaon determines the flavour of the $B^\pm$ and, in the absence of mixing, of the opposite-side B hadron as well. The mistag probabilities are parametrised separately for muons and electrons with analytic functions of the MLP-NN discriminators in order to provide a per-event value of the predicted mistag probability ω. The functional forms of the parametrisations are obtained from the simulated B_s^0 sample. The candidate $B^\pm$ mesons are required to pass the same selection criteria as possible of the signal B_s^0 candidates. The tagging efficiency evaluated by the $B^\pm$ sample is $(4.56 \pm 0.02)\%$ and $(3.92 \pm 0.02)\%$ for muons and electrons, respectively. The mistag parametrisation as a function of the MLP-NN output are shown in Fig. 1 for simulated $B^\pm$ and B_s^0 samples as well as for $B^\pm$ reconstructed data sample. The overall tagging power of the opposite side lepton tagger, measured with a sample of $B^\pm$ events, is $\varepsilon_{tag}D^2 = (1.307 \pm 0.031(\text{stat}) \pm 0.007(\text{syst}))\%$, where $D = (1-2\omega)$ is called "dilution". .

An unbinned maximum-likelihood fit to the data is performed by including the information of the B_s^0 invariant mass ($m_{B_s^0}$), the three decay angles (Θ) of the reconstructed B_s^0 candidates, the

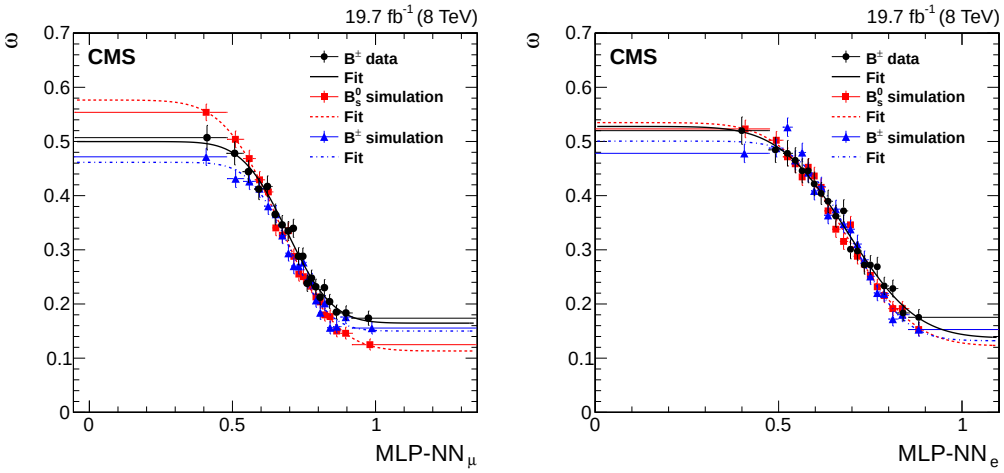

Figure 1: The mistag probabilities ω, defined as the ratio of the number of wrongly tagged events divided by the total number of tagged events, as a function of the MLP-NN discriminators for muons (a) and electrons (b). The data points (solid markers) are placed at the average weighted value of the events in each bin. The vertical bars show the statistical uncertainties and the horizontal bars the bin width. The solid line represents the parametrisation curve extracted from the background-subtracted $B^{\pm}$ data; the dashed and dot-dashed lines refer to the parametrisations extracted from the simulated B_s^0 and $B^{\pm}$ samples, respectively.[3]

flavour tag decision (ξ), ct, and σ_{ct}. The fit is applied to a sample fo about 70 thousand events selected in the mass range from 5.24 to 5.49 GeV and ct between 200 μm and 3 mm, of which 5650 are tagged. From this fit the physics parameters of interest are obtained: $\Delta\Gamma_s, \phi_S$, the mean lifetime $\tau, \Delta m_s, |A_0|^2, |A_\perp|^2, |A_\parallel|^2, |A_S|^2$, and the strong phases $\delta_\parallel, \delta_\perp, \delta_{S\perp}$ where $\delta_{S\perp}$ is defined as the difference $\delta_S - \delta_\perp$.

The likelihood function is composed of probability density functions (pdf) describing the signal and background components. The signal and background pdfs are formed as the product of pdfs that model the invariant mass distribution and the time-dependent decay rates of the reconstructed candidates.

$$\mathscr{L} = N_s \left[f(\Theta, ct, \alpha) \otimes G(ct, \sigma_{ct}) \varepsilon(\Theta) \times P_s(m_{B_s^0}) P_s(\sigma_{ct}) P_s(\xi) \right] \tag{2.4}$$

$$+ N_{bkg} \left[P_{bkg}(\Theta) P_{bkg}(ct) P_{bkg}(m_{B_s^0}) P_{bkg}(\sigma_{ct}) P_{bkg}(\xi) \right] \tag{2.5}$$

where the first term is the pdf that describes the $B_s^0 \to J/\psi\phi$ signal, and the second is the one describing the background. N_s (N_{bkg}) is the number of the signal (background) events, f the decay rate function, G the per event proper decay length resolution function, $\varepsilon(\Theta)$ the angular efficiency function, taken from the Monte Carlo (MC) simulation , and $P_{s(bkg)}(m_{B_s^0}) P_{s(bkg)}(\sigma_{ct}) P_{s(bkg)}(\xi)$ the signal (background) pdf for the mass, proper decay length error and tag decision respectively. The average proper decay length (PDL) uncertainty is 23.4 μm. The systematic uncertainties due to the angular resolutions (that are not included in the fit model) and deviations from flat PDL efficiency are taken as systematics. The fit results are shown in Table 2.

Table 2: Results of the fit to the data. Uncertainties are statistical only.

Parameter	Fit result
ϕ_s [rad]	-0.075 ± 0.097
$\Delta\Gamma_s$ [ps^{-1}]	0.095 ± 0.013
$\lvert A_0\rvert^2$	0.510 ± 0.005
$\lvert A_S\rvert^2$	$0.012^{+0.009}_{-0.007}$
$\lvert A_\perp\rvert^2$	0.243 ± 0.008
$\delta_\parallel$ [rad]	$3.48^{+0.07}_{-0.09}$
$\delta_{S\perp}$ [rad]	$0.37^{+0.28}_{-0.12}$
$\delta_\perp$ [rad]	2.98 ± 0.36
$c\tau$ [μm]	447.2 ± 2.9

Systematic uncertainties are investigated by testing the various assumptions made in the fit model and those associated with the fit procedure. The most relevant ones for the weak phase are: the angular efficiencies, evaluated by propagating the parameters extracted from the simulation within their statistical uncertainties; the small discrepancy of the kaon p_T spectrum between the simulation and the data, evaluated by reweighing the simulated spectrum to the one in data; the model bias, evaluated by using simulated pseudo-experiments; and finally the hypothesis that the direct CP violation has been set to be null evaluated by leaving it float in the fit.

The measured values for the weak phase ϕ_s and the decay width difference $\Delta\Gamma_s$ have been measured to be [3]:

$$\phi_s = -0.075 \pm 0.097(\text{stat}) \pm 0.031(\text{syst}) \text{ rad} \tag{2.6}$$

$$\Delta\Gamma_s = 0.095 \pm 0.013(\text{stat}) \pm 0.007(\text{syst}) \text{ ps}^{-1} \tag{2.7}$$

The corresponding contour plot is shown in Fig 2.

3. Prospects

The published measurement reported in the previous Section will be soon updated with the analysis of the Run2 data. Besides the larger LHC centre-of-mass energy (13 TeV instead of 8 TeV), almost doubling the B hadron production cross-section, and a larger integrated luminosity, in 2017 CMS has installed a new vertex pixel detector allowing for a lower material budget than the previous, a smaller inner radius, and an additional fourth layer, to increase high precision tracking. The increased cross section and the larger instantaneous luminosity, though, have increased the pileup from an average of 16 in Run1 to about 37 in Run2, thus requiring to increase the trigger thresholds, hence a slightly smaller increase in the number of events is expected compared to the simple scaling. Figure 3 shows the proper decay length uncertainty for the Run1 (left) on $B^0_s \to J/\psi\phi$ data, compared to the Run2 (right) $B^0 \to J/\psi K^{*0}$, although with higher momentum selection.

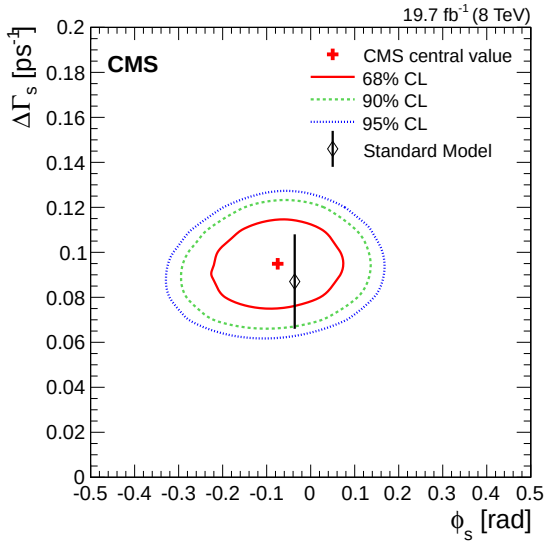

Figure 2: The CMS measured central value and the 68%, 90%, and 95% CL contours in the $\Delta\Gamma_s$ versus ϕ_s plane, together with the SM prediction. Uncertainties are statistical only.[3]

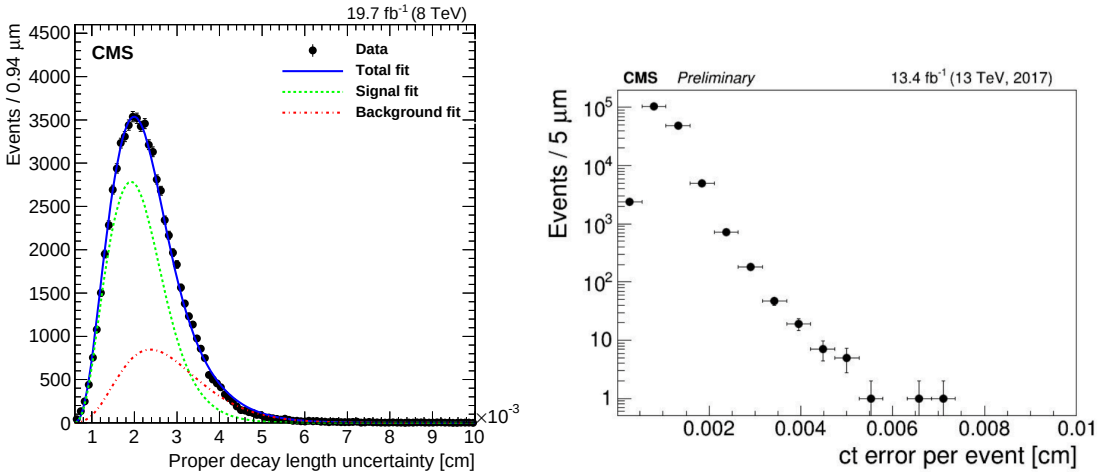

Figure 3: Comparison between the proper decay length uncertainty for the Run1 (left) [3] and Run 2 (right) [5] .

In the High-Luminosity phase of LHC (also known as "Phase-2") the CMS detector will undergo a major upgrade to cope with increased instantaneous luminosities yielding up to 200 pileup events per bunch crossing [6]. In particular, a new tracker system [7] will be build with improved granularity and lower material budget and a wider detector acceptance (up to pseudorapidity 4 instead of the actual one limited to 2.4) and the ability to reconstruct tracks at the first trigger level (L1) for those with transverse momenta above 2 GeV. An improved muon system [8] with extended forward coverage, and a better timing and trigger capability, and finally a timing detector [9] able to reconstruct tracks with about 30 ps resolution. The first two new tracking apparata (tracker and

muon system) will allow to increase the efficiency and the resolution of the reconstructed B_s^0, as shown in Fig. 4. The timing detector will allow discriminating the Kaons from pions up to about 2 to 3 GeV momenta, depending on the polar angle.

CMS has estimated the expected sensitivity on the CP-violating phase ϕ_s the end of the HL-LHC data-taking with 3 ab^{-1} of collected data [10]. To study the expected detector performance in Phase 2, a dedicated Monte Carlo sample generated with a centre-of-mass energy of 14 TeV and ideal Phase-2 detector conditions is used.

The new L1 trigger capability to reconstruct charged tracks above 2 GeV in transverse momentum with almost offline-like resolutions, will be able to provide a clean J/ψ sample. Preliminary studies of the transverse impact parameter reconstruction at L1 indicate a resolution between 100 and 300 μm, which can be used to reduce the prompt J/ψ component at L1 if needed. The Phase 2 L1 (hardware) and HLT (software) trigger performances are expected to be comparable to those during Run2, and sustainable in terms of rates. The offline selections could therefore be identical to those used in the 2012 data analysis and CMS assumes no difference in the signal over background ratio with respect to 2012 data.

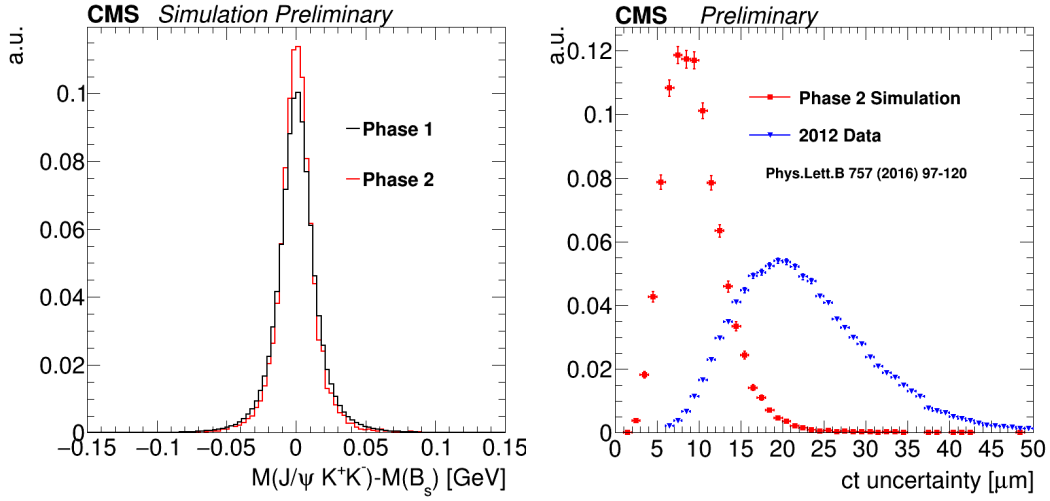

Figure 4: Left: invariant mass resolution in the Phase 2 sample compared with Phase 1 case. Right: proper time uncertainty distribution in 2012 data (blue) and Phase 2 MC (red) samples. The better performance of Phase 2 w.r.t. 2012 data is due to the Phase 2 tracker.

The expected sensitivity for Phase 2 is estimated using the toy MC pseudo-experiment technique. A set of toy MC samples is generated using the signal model of $B_s^0 \to J/\psi\phi$ decay described in the previous Section. Each sample consists of about 9 million signal events, corresponding to the expected yield after 3 ab^{-1} of integrated luminosity, which is a conservative assumption based on 2012 and 2018 data rates. The proper decay length uncertainty is estimated using a MC signal sample with a GEANT4 simulation of an ideal Phase 2 detector response (Fig. 4). The flavour tagging dilution is included in the toy MC production by fixing it to its "effective" value (the constant value of the dilution which reproduces the same effect on the ϕ_s accuracy of the per-event dilution). The generated toy MC samples are fitted using the same signal model used for their production. The fit extracts ϕ_s and $\Delta\Gamma_s$ for each toy experiment. The resulting ϕ_s uncertainty distribution is fitted using

a Landau function and the most probable value is used to determine the sensitivity on ϕ_s for the set of toy MC samples. The uncertainty on ϕ_s in the 2012 data CMS analysis is driven by the statistical uncertainty. The main systematic which affected the 2012 result will be reduced by improving the MC statistics for the angular efficiency calculations and by optimising and improving the fit model. Similarly, the flavour tagging systematics (that accounted for 3 mrad in 2012) will benefit of larger calibration sample thus reducing its impact considerably to less than 1 mrad, reasonably.

In order to evaluate the CMS capability on ϕ_s CMS has tested three scenarios, depending on the flavour tagging performance that will ultimately be achieved. A conservative one (scenario *a*) is represented by a tagger based on a combination of opposite side muons and jet-charge; a second scenario (*b*) is only considering opposite side electrons and muons as in the 2012 analysis, while a third scenario (*c*) is the one which combines opposite side leptons (electrons and muons) with the opposite and same side jet-charge/kaon tagging. The results are summarised in Fig. 5. The sensitivity on ϕ_s will be limited by the statistical error, ranging from about 4.5 to 5.5 mrad depending on the proposed flavour tagging scenario.

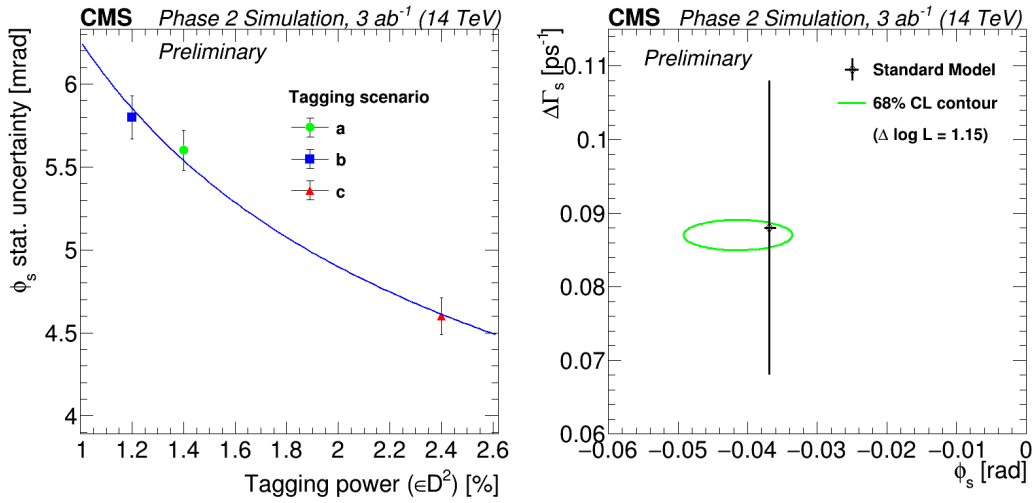

Figure 5: Left: variation of the ϕ_s statistical uncertainty as function of the tagging power (εD^2), measured in different flavour tagging scenarios. Right: 68% confidence level (CL) contour from the fit of a toy MC pseudo-experiment generated in the tagging scenario *c*. The contour combines statistical and systematic uncertainties. The black cross represents the SM expectations .

Finally a combination of expected Phase 2 results from CMS, ATLAS and LHCb has been performed [11] and compared with the current experimental limit and is reported in Fig. 6.

4. Conclusions

CMS has measured the weak phase ϕ_s with 19.7 fb^{-1} of data at $\sqrt{s} = 8$ TeV. The measurement is in agreement with the Standard Model prediction. CMS is currently working in analysing Run2 data, with increased statistics and improved proper time resolution, thanks to a better pixel detector installed in 2017. In the HL-LHC phase CMS will undergo into a major detector upgrade that will allow to improve the proper time resolution and the trigger efficiencies, thus exploiting the full

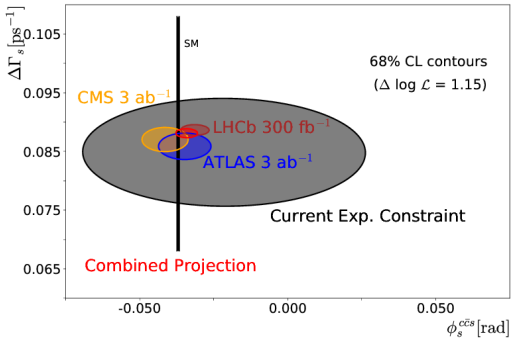

Figure 6: Projected 68% confidence-level contour in the $\Delta\Gamma_s$ vs ϕ_s plane for the ATLAS, CMS and LHCb sensitivity at the HL-LHC compared with the current experimental limit (from Reference [11]).

expected statistics of 3 ab^{-1}; the expected reach in the ϕ_s sensitivity is about 5 mrad, limited by the statistical error.

Acknowledgments

I would like to thank the organisers of the Conference for the beautiful venue and relaxed atmosphere.

References

[1] S. Faller, R. Fleischer, and T. Mannel, Phys. Rev. D 79 (2009) 014005, doi:10.1103/PhysRevD.79.014005

[2] J. Charles et al., Phys. Rev. D84, 033005 (2011), updated with Summer 2019 results (http://ckmfitter.in2p3.fr/www/results/plots_summer19/num/ckmEval_results_summer19.pdf)

[3] CMS Coll., Phys. Lett. B 757 (2016), 97-120, https://doi.org/10.1016/j.physletb.2016.03.046

[4] A. S. Dighe, I. Dunietz, H. J. Lipkin, and J. L. Rosner, Phys. Lett. B 369 (1996) 144, doi:10.1016/0370-2693(95)01523-X

[5] CMS Coll. CMS DP -2018/027, http://cds.cern.ch/record/2622156/.

[6] CMS Coll., Technical Report CERN-LHCC-2015-010, LHCC-P-008. CMS-TDR-15-02-, 2015.

[7] CMS Coll., Technical Report CERN-LHCC-2017-009. CMS-TDR-14, 2017.

[8] CMS Coll., Technical Report CERN-LHCC-2017-012. CMS-TDR16, 2017.

[9] CMS Coll., Technical Report CERN-LHCC-2019-003 ; CMS-TDR-020, 2019.

[10] CMS Coll., CMS PAS FTR-18-041, https://cds.cern.ch/record/2650772.

[11] A. Cerri et al. CERN Yellow Reports: Monographs, [S.l.], v. 7, p. 867, dec. 2019. ISSN 2519-8076. doi:http://dx.doi.org/10.23731/CYRM-2019-007.867.